DOI: 10.1002/chem.200801304

# Three-Dimensional Ultralarge-Pore *Ia3d* Mesoporous Silica with Various Pore Diameters and Their Application in Biomolecule Immobilization

**Ajayan Vinu,*[a] Narasimhan Gokulakrishnan,[a] Veerappan V. Balasubramanian,[a] Sher Alam,[a] Mahendra P. Kapoor,[b] Katsuhiko Ariga,[a] and Toshiyuki Mori[c]**

**Abstract:** Highly ordered mesoporous three-dimensional *Ia3d* silica (KIT-6) with different pore diameters has been synthesized by using pluronic P123 as surfactant template and *n*-butanol as cosolvent at different synthesis temperatures in a highly acidic medium. The materials were characterized by XRD and $N_2$ adsorption. The synthesis temperature plays a significant role in controlling the pore diameter, surface area, and pore volume of the materials. The material prepared at 150 °C, KIT-6-150, has a large pore diameter (11.3 nm) and a high specific pore volume (1.53 $cm^3 g^{-1}$). We also demonstrate immobilization of lysozyme, which is a stable and hard protein, on KIT-6 materials with different pore diameters. The amount of lysozyme adsorbed on large-pore KIT-6 is extremely large (57.2 $\mu mol g^{-1}$) and is much higher than that observed for mesoporous silicas MCM-41, SBA-15, and KIT-5, mesoporous carbons, and carbon nanocages. The effect of various parameters such as buffer concentration, adsorption temperature, concentration of the lysozyme, and the textural parameter of the adsorbent on the lysozyme adsorption capacity of KIT-6 was studied. The amount adsorbed mainly depends on solution pH, ionic strength, adsorption temperature, and pore volume and pore diameter of the adsorbent. The mechanism of adsorption on KIT-6 under different adsorption conditions is discussed. In addition, the structural stability of lysozyme molecules and the KIT-6 adsorbent before and after adsorption were investigated by XRD, nitrogen adsorption, and FTIR spectroscopy.

**Keywords:** adsorption · hydrothermal synthesis · immobilization · mesoporous materials · silica

## Introduction

Adsorption of proteins on solid surfaces has been a topic of interest in recent years and plays a critical role in various applications including the formulation and stabilization of foam- and emulsion-based products in the food industry, analysis and purification of proteins, preparation of immunoassays for medical diagnostic tests, enzymatic catalysis, drug-delivery systems, and protein-based biosensors.[1–18] Further advances in the above applications require in-depth knowledge of the basics of protein adsorption on different solid adsorbents, and the factors affecting the amount of protein adsorbed and the structure and stability of the protein after adsorption. The adsorption behavior of proteins over various nonporous solid substrates such as silica and mica has been studied by methods such as in situ ellipsometry,[19] neutron reflection,[20] fluorescence with total internal reflection,[21] UV absorbance[22] and time-resolved optical waveguide light-mode spectroscopy (OWLS).[23–25]

Porous materials such as zeolites and zeotype materials have received much attention owing to their application in adsorption and separation of small organic molecules.[26–27] Although zeolites and zeotype materials have huge surface areas and large pore volume, and proved to be efficient adsorbents for small organic molecules, they are not suitable

[a] Dr. A. Vinu, Dr. N. Gokulakrishnan, Dr. V. V. Balasubramanian, Dr. S. Alam, Dr. K. Ariga
International Center for Materials Nanoarchitectonics
Word Premier International (WPI) Research Center
National Institute for Materials Science
1-1, Namiki, Tsukuba, 305-0044 (Japan)
Fax: (+81) 29-860-4563
E-mail: vinu.ajayan@nims.go.jp

[b] Dr. M. P. Kapoor
Taiyo Kagaku Co. Ltd.
Research&Development
Interface Solution Division
1-3 Takaramachi, Yokkaichi, Mie 510-0844 (Japan)

[c] Dr. T. Mori
Nano-ionics Materials Group
National Institute for Materials Science
1-1, Namiki, Tsukuba, 305-0044 (Japan)

   

for the adsorption of large biomolecules such as proteins and enzymes. This is mainly due to their micropore size, which limits the diffusion of the large biomolecules inside the pore channels and access to the adsorption sites. To overcome these problems, adsorption of proteins has been studied over sol–gels and controlled porous glass (CPG), the pores of which are much larger than protein molecules.[9,15,18] However, sol–gels have broad pore size distributions, which are disadvantageous for selective removal of protein molecules with different sizes. Moreover, the preparation of the sol–gels involves harsh conditions or reagents which may harm the nature, stability, and the activity of the proteins. On the other hand, CPGs offer high selectivity in the adsorption of large biomolecules, but their high cost and lower surface area make them unsuitable for adsorption of proteins.

The surfactant-templated self-assembly approach has generated mesoporous materials with different structures.[28–30] Generally, ordered mesoporous materials have excellent properties such as surface area, pore volume, large and tunable pore diameters, well-defined porous structure, and excellent morphologies, which have helped them to find many applications such as catalysis, adsorption, sensing, drug delivery, and separation.[29–42] Balkus et al. were the first to exploit the large pore diameter of mesoporous materials for immobilization of biomolecules such as proteins and enzymes.[35] Recently, Vinu et al. investigated the factors affecting the extent of protein adsorption on one-dimensional mesoporous silica and carbon materials with different pore diameters and found that the loading efficiency of mesoporous materials depend on the pore size, pore volume, and surface charge of the adsorbent, the protein concentration, and adsorption conditions such as solution pH and the equilibration time.[36–42]

Mesoporous silicas with three-dimensional porous networks are thought to have advantages over materials having one-dimensional arrays of pores, mainly because materials with three-dimensional pore structure are more resistant to pore blocking, have better mass transfer of the reactant molecules in the pore channels, and provide more adsorption sites. However, only a few reports are available on immobilization of biomolecules such as cytochrome c and lysozyme on three-dimensional mesoporous materials such as KIT-5, KIT-5-130, and KIT-5-150.[34,43] Although KIT-5 materials have three-dimensional cage-type structures, they show poor protein adsorption capacity, mainly due to their small pore volume. Recently, Ryoo et al. reported a three-dimensional large-pore mesoporous silica with cubic *Ia3d* symmetry (KIT-6), which has well-ordered pore structure with high surface area, large pore volume, and large, tunable pore diameters. KIT-6 was synthesized by utilizing an ethylene oxide (EO) propylene oxide (PO) triblock copolymer ($EO_{20}PO_{70}EO_{20}$)/butanol mixture as structure-directing agent in a highly acidic medium.[44] The materials are of interest for their three-dimensional structures with large pore diameters. The pore diameter of KIT-6 is similar to that of SBA-15 but larger than that of MCM-48. The pore diameter of the materials can also be tuned by simply changing the synthesis temperature. Although the structure and textural parameters of the KIT-6 materials are superior to those of MCM-48, no detailed study has been performed on immobilization of biomolecules on these materials.

Here we report on the preparation and characterization of KIT-6 materials with different pore diameters by using pluronic P123 surfactant in a highly acidic medium at different synthesis temperatures. A synthesis temperature of 150 °C gave KIT-6 materials with large pore diameter and large pore volume. We also demonstrate immobilization of lysozyme, which is a stable and hard protein with molecular dimensions of $3.0\times4.5\times3.0$ nm, a molecular mass of 14400 Da, and an isoelectric point of 10.5,[45] on KIT-6 materials with different pore diameters. The amount of lysozyme adsorbed on large-pore KIT-6 of 57.2 $\mu mol\,g^{-1}$ is the highest value reported for mesoporous materials so far. The effect of various parameters such as buffer concentration, adsorption temperature, concentration of lysozyme, and the textural parameters of KIT-6 on the lysozyme adsorption capacity was studied in detail. The extent of adsorption mainly depends on the solution pH, ionic strength, adsorption temperature, and pore volume and pore diameter of the adsorbent. The structural stability of lysozyme molecules and the KIT-6 adsorbent before and after adsorption measurements were confirmed by physiochemical methods such as XRD, $N_2$ sorption, and FT-IR spectroscopy.

## Results and Discussion

**Characterization of KIT-6 materials with different pore diameters**: The synthesis temperature was varied from 100 to 150 °C to control the pore diameter and the pore volume of the KIT-6 materials. The quality and phase purity of samples prepared at different temperature were assessed by powder XRD measurements. Figure 1 shows the powder XRD diffraction patterns of KIT-6-100, KIT-6-130, and KIT-6-150. All samples exhibit a sharp, well-resolved (211) reflection and several higher order reflections at $2\theta$ value between 3 and 5°, which indicate excellent structural ordering with the

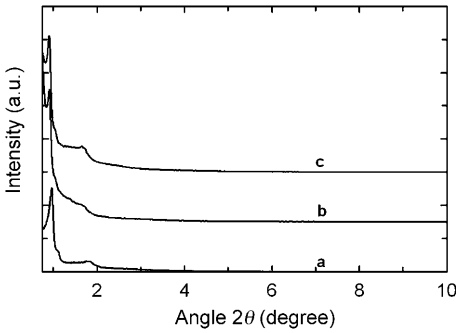


Figure 1. Powder XRD patterns of a) KIT-6-100, b) KIT-6-130, and c) KIT-6-150.

  

symmetry of the body-centered cubic space group *Ia3d*, and the XRD patterns are similar to those of previously reported KIT-6 materials.[44] The cubic *Ia3d* symmetry in all the samples is further confirmed by the fact that the reciprocal of the *d* spacings of the samples prepared at different temperature has a linear relationship with the square root of the sum of $h^2$, $k^2$, and $l^2$. The much higher intensity of the sharp peak in the XRD patterns of the samples prepared at 130 and 150 °C compared to the sample prepared at 100 °C indicates enhanced condensation of silanol groups in the mesoporous wall structure and improved long-range ordering of samples prepared at higher temperature. Increasing the synthesis temperature of the samples causes a shift of the (211) XRD reflection to lower $2\theta$, which reflects an increase in the *d* spacings and unit-cell constants of the samples. The unit-cell constants of KIT-6-100, KIT-6-130, and KIT-6-150, calculated from the (211) reflection of the cubic *Ia3d* space group as $d_{211}\sqrt{6}$, are 22.5, 23.6, and 24.0 nm, respectively. These results indirectly reveal that the pore diameter of the KIT-6 materials also increases with increasing synthesis temperature.

The effect of the synthesis temperature on the porous structure and the topology of the materials was studied by HRTEM. The HRTEM images of KIT-6-100 and KIT-6-150 are shown in Figure 2. The bright lines correspond to pore walls, and dark portions of the images to pore channels. The side-view HRTEM images (Figure 2 A and B) of both the samples show well-ordered pore structure with a linear array of pores arranged at regular intervals. The orientation and pore entrance of the individual pores are clearly visible in the top-view HRTEM images of both samples (Figure 2 C and D). The HRTEM images also provide evidence for the presence of a three-dimensional cubic structure with channels running along the different pore directions, similar to that reported for KIT-6. Significantly, the HRTEM images also reveal that the pore diameter of KIT-6-150 is much larger than that of KIT-6-100, which is consistent with the pore diameters obtained by nitrogen sorption measurements (Table 1).

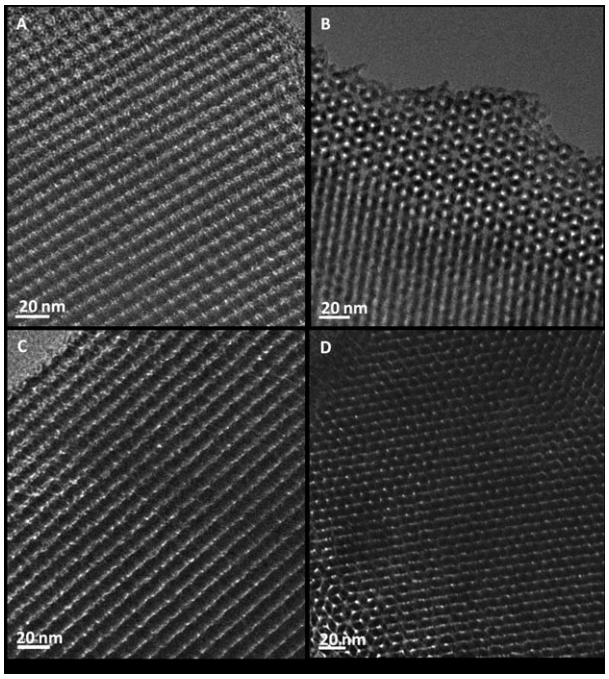


Figure 2. HRTEM images of a, b) KIT-6-100 and c, d) KIT-6-150.

Table 1. Structural characteristics of KIT-6.

| Material | $d_{211}$ spacing [nm] | Unit cell $a_0$ [nm] | $A_{BET}$ [$m^2 g^{-1}$] | $V_p$ [$cm^3 g^{-1}$] | $d_{p,BJH}$ [nm] |
|---|---|---|---|---|---|
| KIT-6-100 | 9.17 | 22.5 | 728 | 0.99 | 8.0 |
| KIT-6-130 | 9.62 | 23.6 | 625 | 1.32 | 9.9 |
| KIT-6-150 | 9.81 | 24.0 | 555 | 1.53 | 11.3 |

Low-temperature nitrogen adsorption/desorption measurements were used to calculate the specific surface area, pore size distribution, and specific pore volume of the KIT-6 materials. The nitrogen adsorption isotherms and the textural parameters of the KIT-6 materials prepared at different temperatures are shown in Figure 3 and Table 1, respectively. All the samples display type IV isotherms. The presence of a sharp capillary condensation or evaporation step at higher relative pressure and H1 hysteresis loop indicate that all the materials have a uniform pore structure with large channel-like mesopores. When the synthesis temperature is increased from 100 to 150 °C, the capillary-condensation region of the isotherm, which gives information about the pore diameter of the materials, shifts to higher relative pressure. This indicates that the pore diameter of the materials indeed increases with increasing synthesis temperature, consistent with the increase in unit-cell size observed in the XRD patterns (Table 1). The synthesis temperature also has a significant impact on textural parameters of the materials such as specific surface area and specific pore volume. When the synthesis temperature is increased from 100 to 150 °C, the specific surface area of the materials decreases from 728 to 555 $m^2 g^{-1}$, but the specific pore volume and pore diameter increase from 0.99 to 1.53 $cm^3 g^{-1}$, and 8.0 to

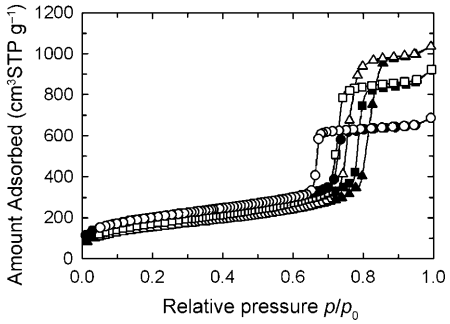


Figure 3. Nitrogen adsorption–desorption isotherms of KIT-6 materials prepared at different temperature (closed symbols: adsorption; open symbols: desorption): ● KIT-6-100, ■ KIT-6-130, ▲ KIT-6-150.

  

11.3 nm, respectively. The material prepared at the synthesis temperature of 150 °C, KIT-6-150, has a large pore diameter and high specific pore volume, but its adsorption pore size distribution is broader than those of KIT-6-130 and KIT-6-100 (Figure 4).

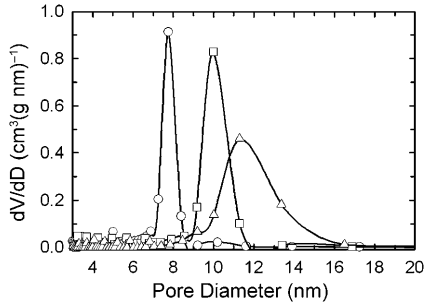


Figure 4. BJH pore size distribution of KIT-6 materials prepared at different temperatures: ○ KIT-6-100, □ KIT-6-130, △ KIT-6-150.

The effect of the synthesis temperature on the pore diameter of the KIT-6 materials can be explained by changes in the nature of the block copolymer with temperature. At low temperature, the poly(ethylene oxide), PEO, chains of the micelle are hydrophilic, and the poly(propylene oxide), PPO, chains are hydrophobic. These PEO chains penetrate into the walls of KIT-6 and interact with the silanol groups by hydrogen bonding. When the synthesis temperature is increased from 100 to 150 °C, the hydrophilicity of the PEO chains decreases with a concomitant increase in hydrophobic character. We believe that the increased hydrophobic character enhances the interaction between the PPO and PEO chains of the micelle. As a result, the length of the hydrophobic part of the surfactant micelle increases (interaction between PEO and PPO chains), and thus the micelle size increases with increasing synthesis temperature. The increase in micelle size, which generally determines the pore diameter of mesoporous materials, is responsible for the enlarged pore diameter of the KIT-6 materials synthesized at high temperature. However, broadening of the pore size distribution of KIT-6-150 is attributed to differences in micelle size at very high temperature due to breakage of the large micelles.

**Immobilization of lysozyme molecules inside the mesochannels of KIT-6**: KIT-6 materials with different pore diameters and the specific pore volumes were used for the adsorption of lysozyme molecules from buffer solution. As the lysozyme molecule is relatively large, long equilibration times are needed. From our previous studies, we found that at least 96 h is required to reach the adsorption equilibrium of lysozyme molecules on the large pore mesoporous SBA-15 silica.[37] Thus, an adsorption time of 96 h was used in all adsorption experiments conducted in this work.

**Influence of pore volume and pore diameter on the adsorption of lysozyme on KIT-6**: To study the role of the textural parameters of the adsorbent on the amount of lysozyme adsorbed in the porous channels, adsorption parameters such as solution pH, buffer (phosphate) concentration (25 mM), and adsorption temperature (20 °C) were kept constant. Figure 5 shows the adsorption isotherms of lysozyme on

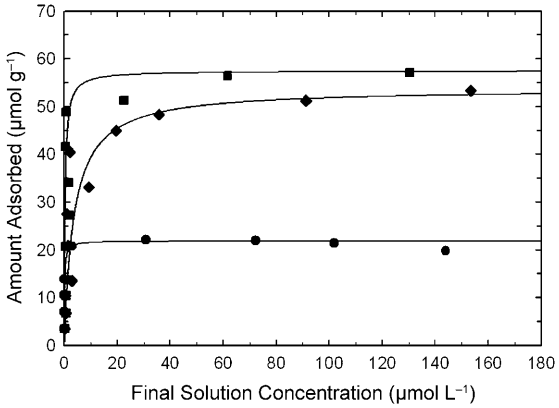


Figure 5. Adsorption isotherms of lysozyme on KIT-6 with various pore diameters: ● KIT-6-100, ◆ KIT-6-130, and ■ KIT-6-150. Buffer concentration 25 mM, adsorption temperature 25 °C, solution pH 11.0.

KIT-6 with different pore diameters and pore volumes, wherein the amount of lysozyme adsorbed per unit weight of adsorbent is plotted against equilibrium concentration of the lysozyme solution. The adsorption equilibrium data were fitted by using the Langmuir model, which assumes monolayer coverage of the adsorbent, and the solid lines in the Figure 5 are the best fit Langmuir isotherm obtained from Equation (1),

$$n_s = Kn_m c/(1 + Kc)$$

where $K$ is the Langmuir constant, $c$ the lysozyme concentration, $n_m$ the monolayer adsorption capacity, and $n_s$ the amount of lysozyme adsorbed on the adsorbent. All of the isotherms are of L type according to the Giles classification.[46] Each isotherm shows a sharp initial rise indicating a high affinity between lysozyme and the adsorbent surface. With increasing lysozyme concentration in the buffer solution, the amount of lysozyme adsorbed on the porous surface of the KIT-6 adsorbent increases. Finally, when the initial lysozyme concentration is increased to 5 g $L^{-1}$, all of the isotherms reach a plateau. Monolayer adsorption capacity increases with increasing the pore diameter and pore volume of the KIT-6 adsorbents (Figure 5, Table 1). KIT-6-150 has a very high lysozyme adsorption capacity of 57.2 μmol $g^{-1}$, which is much higher than those of 22.1 μmol $g^{-1}$ and 53.3 μmol $g^{-1}$ for KIT-6-100 and KIT-6-130, respectively. This could be due to the fact that the pore diameter and pore volume of KIT-6-150 are much larger than those of KIT-6-100 and KIT-6-130.

The effect of the pore diameter and pore volume of KIT-6 adsorbents on the rate of the lysozyme adsorption was also studied. Information about the rate of adsorption of

  

proteins on the surface of the adsorbents is important for separation and chromatographic applications. The three-dimensional structure of KIT-6 may help to achieve excellent mass transfer of the adsorbate molecule and achieve high adsorption capacity in a short time. Figure 6 shows the rate

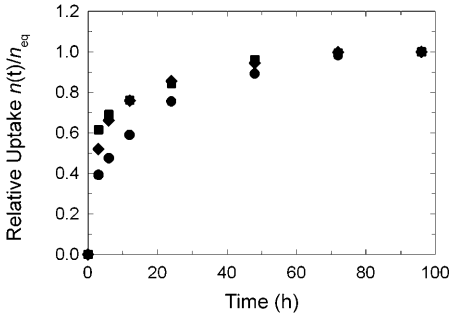


Figure 6. Relative uptake $n(t)/n_{eq}$ versus $t$ at pH 11. Buffer concentration 25 mM, adsorption temperature 25 °C, concentration of lysozyme 5 g $L^{-1}$. ● KIT-6-100, ◆ KIT-6-130, and ■ KIT-6-150.

of lysozyme adsorption, expressed as $n(t)/n_{eq}$ ($n_{eq}$ = amount lysozyme adsorbed on KIT-6 adsorbents at thermodynamic equilibrium) versus adsorption time $t$. With increasing adsorption time, the amount of lysozyme adsorbed also increases. At an adsorption time of 3 h, KIT-6-150 shows almost two times higher rate of adsorption than KIT-6-100. From the rate of adsorption data, it can also be deduced that the time required to reach 85 % of the equilibrium adsorption is 24 h for KIT-6-150, whereas 48 h are required to reach the same amount of adsorption in KIT-6-100. This clearly indicates that the small pore diameter of the KIT-6-100 may cause space constraints and restrict the access of free adsorbate molecules to vacant adsorption sites in the internal porous structure, and thus a long time is required for adsorption of lysozyme molecules. From these results, it can be concluded that the pore diameter and pore volume of the KIT-6 adsorbent play a significant role in controlling the amount and rate of lysozyme adsorption in the mesoporous channels of the adsorbents.

The superiority of KIT-6-150 in lysozyme adsorption is demonstrated by comparing its adsorption data with those of other mesoporous materials such as MCM-41, KIT-5, and SBA-15 under the same adsorption conditions. The lysozyme capacity decreases in the following order: KIT-6-150 > KIT-6-130 > SBA-15-100 > C16-MCM-41 > C12-MCM-41 > KIT-5-150. The monolayer adsorption capacities of SBA-15-100, C16-MCM-41, C12-MCM-41, and KIT-5-100 are 35.3, 28.1, 13.4, and 5.2 μmol $g^{-1}$, respectively.[34,37,43] Although KIT-5 has a three-dimensional porous structure with the pore size (ca. 4.0 nm) which is similar to the size of the lysozyme molecule, it shows the least adsorption capacity for lysozyme (5.16 μmol $g^{-1}$).[43] This is contrary to the expectation for three-dimensional materials, and further reveals that, other than the structure, another parameter is also involved in controlling protein adsorption. As reported previously, the specific pore volume of KIT-5 is around 0.44 $cm^3 g^{-1}$, which is much lower than those of the other mesoporous materials used in the adsorption study (Table 1). Thus, we surmise that the lower adsorption capacity of KIT-5 is solely due to its poor textural characteristics. On the other hand, the lysozyme adsorption capacity of KIT-6-150 of 57.2 μmol $g^{-1}$ is the highest ever reported for mesoporous materials and is almost 2, 3, and 10 times higher than those of SBA-15, MCM-41, and KIT-5-100, respectively.

The adsorption capacity of KIT-6-150 is also larger than those of mesoporous carbons (22.9 μmol $g^{-1}$, CMK-3-150) and carbon nanocages (26.5 μmol $g^{-1}$, CNC).[38,38] This high adsorption capacity of KIT-6-150 could be mainly due to its large pore volume and pore diameter. Another possible explanation is that KIT-6 has a three-dimensional large-pore network with two nonintersecting pore systems which allows adsorbate molecules to access the adsorption sites from all the three directions. As a result, a huge adsorption capacity for the lysozyme molecule is observed. From these results, it can be concluded that a good adsorbent for biomolecules should not only have a large pore diameter, which provides free access to the adsorption sites, but also a large specific pore volume of the adsorbent, which is required to accommodate a large quantity of biomolecules in the mesoporous channels, and a well-ordered three-dimensional structure for easy access of the adsorbate molecules.

**Influence of pH**: Besides the textural parameters of the KIT-6 materials, the solution pH is another critical factor for protein adsorption, as it significantly affects the degree of ionization of the functional groups on the surface of the proteins and the surface charge of the adsorbents. Therefore, we investigated the effect of solution pH on the extent of lysozyme adsorption on KIT-6 materials. These studies are important because pH change is one of the most common methods used for eluting proteins in immobilized metal ion affinity chromatography. KIT-6-150 was used for this study as it showed the highest degree of lysozyme adsorption. The adsorption isotherms of lysozyme on KIT-6-150 at solution pHs ranging from 6.5 to 12 are plotted in Figure 7. The monolayer adsorption capacity significantly depends on solution pH, and the amount adsorbed increases with increasing solution pH from pH 6.5 to 11, reaches a maximum at pH 11, and then decreases. A similar trend was observed by Vinu et al. for mesoporous silica materials, such as MCM-41 and SBA-15, and mesoporous carbon materials.[36–39] They showed that the hydrophobic interaction and electrostatic repulsion and attraction between the adsorbent and the protein molecule greatly vary with solution pH and significantly influence the amount of lysozyme adsorbed MCM-41 and SBA-15 materials.

The maximum adsorbed amount of 57.2 μmol per gram of KIT-6-150 was registered near the isoelectric point, that is, at a solution pH of 11. At this pH, the net charge of the protein is low, Coulombic repulsive force between and or within the protein molecules would be minimal, and closer packing of the protein molecules is possible. Moreover,

  

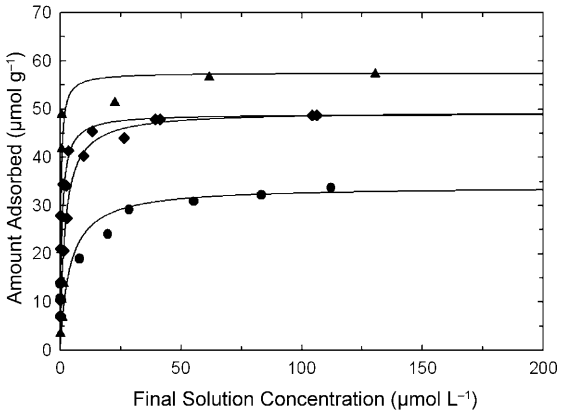


Figure 7. Adsorption isotherms of lysozyme over KIT-6-150 measured at different solution pH: ● pH 6.5, ◆ pH 9.6, ■ pH 11.0, and ▲ pH 12.0. Buffer concentration 25 mM, adsorption temperature 25 °C.

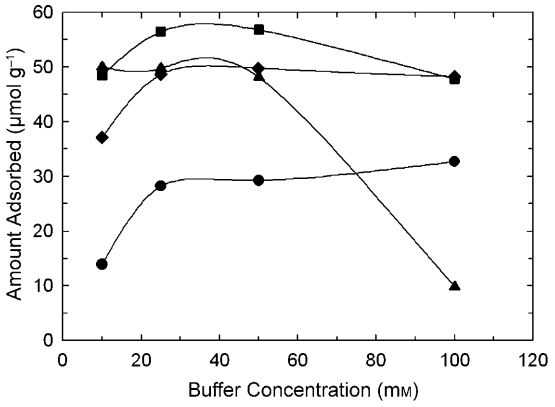


Figure 8. Effect of buffer concentration on the adsorption of lysozyme over KIT-6-150 as a function of solution pH (adsorption temperature 25 °C): ● pH 6.5, ◆ pH 9.6, ■ pH 11.0, and ▲ pH 12.0.

when the pH is close to the isoelectric point of lysozyme, the hydrophobic interactions, which originate from the amido groups on the surface of the lysozyme molecules, and the interaction between the amido groups of lysozyme and the siloxane bridges on the surface of the KIT-6 adsorbent, are dominant and are also responsible for enhanced protein adsorption near the isoelectric point. As a result, maximum adsorption is observed at pH 11. Above and below pH 11, the amount of lysozyme adsorption significantly decreases. The decreased lysozyme adsorption at lower pH is correlated with the increased positive charge on the protein molecules and thus increased hydrophilicity. The increased positive charge on the surface of the protein also implies that the electrostatic repulsion within the molecules will be greater. These factors limit close packing of the lysozyme molecules and lead to a low adsorption capacity. On the other hand, when the solution pH is increased above the isoelectric point, the negative charge on the surface of the lysozyme molecule and the adsorbent start to increase, and so does the electrostatic repulsion between the negatively charged silica surface of KIT-6-150 and the negatively charged lysozyme, and electrostatic repulsion within and/or between the lysozyme molecules is dominant. The combination of these factors hinders adsorption of lysozyme on the silica surface, and thus leads to low adsorption capacity when the pH of the solution is increased above the isoelectric point of lysozyme.

**Influence of ionic strength**: To study the influence of the ionic strength of the buffer, adsorption experiments were carried out at different buffer concentrations and different pH values over KIT-6-150. Figure 8 shows the adsorption of lysozyme on KIT-6-150 as a function of the ionic strength of the buffer with the solution pH in the range of 6.5–12. Adsorption of lysozyme on KIT-6-150 is significantly affected by the ionic strength of the buffer at different solution pH values, and this reveals the presence of a screening effect produced by the different concentrations of phosphate or carbonate ions in the buffer. A marked increase in the amount of adsorbed lysozyme is observed on increasing the ionic strength of the buffer from 10 to 100 mM at a solution pH of 6.5, but a little change is observed when the solution pH is increased further to 9.6. This could be mainly due to the fact that when the solution pH is decreased from 9.6 to 6.5, the charge on the phosphate ions of the buffer increases and so do the repulsive forces between the phosphate ions. As the ionic strength of the buffer increases, the repulsive electrostatic interaction between the phosphate ions in the buffer also increase. These strong repulsive forces push the lysozyme molecules together and enhance the interaction between the positively charged silica surface and the negatively charged lysozyme molecules. Thus, the amount of adsorbed lysozyme also increases with increasing ionic strength of the buffer at a solution pH of 6.5.

However, when the solution pH is further increased to 11, the amount of lysozyme adsorbed increases with increasing ionic strength of the buffer from 10 to 50 mM, but decreases at an ionic strength of 100 mM. At a solution pH of 11, the charge of lysozyme is almost zero and hydrophobic interaction is mainly involved in the adsorption process. The change in the ionic strength of the buffer is expected to promote hydration of carbonate ions, which decreases the solubility of the proteins and favors close packing of protein molecules in the mesochannels. However, when the ionic strength of the buffer is further increased from 50 to 100 mM, the negatively charged carbonate ions form a shield on the surface of the proteins. This would increase the electrostatic repulsion between the negatively charged shielded protein surface and the negatively charged silica surface with concomitant decrease of the hydrophobic interaction between the adsorbent and the protein surface, which is dominant at pH values near the isoelectric point of the protein, and hence adsorption is weak. When the ionic strength of the buffer solution is increased from 10 to 100 mM at a solution pH of 12, a drastic reduction in protein adsorption on the surface of KIT-6-150 is observed. This is mainly due to the fact that as the concentration of the buffer is increased from 10 to 100 mM at higher pH, the negatively charged ions

  

present in the buffer start to shield the surface of the protein and enhance the electrostatic repulsion between the negatively charged adsorbent surface and the protein surface, which leads to formation of large aggregates of lysozyme molecules. These may block the pore entrance of KIT-6-150 and thus reduce the extent of adsorption.

**Influence of temperature**: The influence of temperature on the adsorption of lysozyme on KIT-6-150 is shown in Figure 9. The amount of lysozyme adsorbed on KIT-6-150

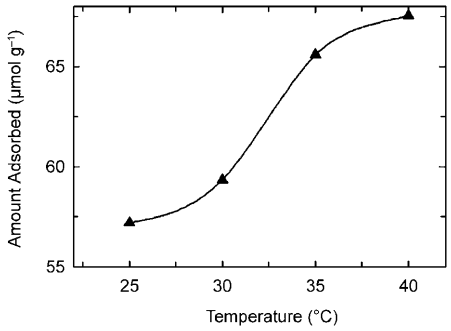


Figure 9. Effect of temperature on the adsorption of lysozyme adsorbed over KIT-6-150. Buffer concentration 25 mM, solution pH 11.0.

increases with increasing adsorption temperature from 20 to 40 °C. This indicates that the adsorption process is endothermic ($\Delta_{ads}H>0$) and entropy-driven.[47] A maximum adsorbed amount of 67.3 μmol $g^{-1}$, which corresponds to around 970 mg $g^{-1}$, was obtained for KIT-6-150 at 40 °C and pH 11. To the best of our knowledge, this is the highest ever reported value for the adsorption of lysozyme on mesoporous materials. Protein conformation varies significantly with temperature and can be partially destroyed at high temperature. This would expose the inner hydrophobic part of the protein molecules to the buffer solution, which could favor strong binding with the adsorbent surface. When the adsorption temperature is increased from 25 to 40 °C, we surmise that some of the lysozyme molecules undergo structural rearrangement to a thermodynamically unstable form that has greater affinity to surface of KIT-6-150 than the thermodynamically stable molecules, which tend to be adsorbed only through electrostatic attraction between protein and surface.[48–49] Moreover, solution polarity also significantly changes with temperature. The decrease in polarity with increasing temperature is also responsible for the increased lysozyme adsorption capacity of KIT-6-150 at high temperature. High temperatures also promote protein unfolding, which can enhance binding with the adsorbent surface and even allow multilayer adsorption.[50,51] Thus, we assume that these combined factors are responsible for the increased lysozyme adsorption on KIT-6-150 on increasing the adsorption temperature.

**Characterization of the adsorbent after lysozyme adsorption**: To check the structural stability of the adsorbent before and after adsorption, and whether the lysozyme molecules are immobilized inside the mesoporous channels or on the external surface, the KIT-6-150 materials before and after immobilization of lysozyme at two different concentration were evaluated by powder XRD measurements and nitrogen adsorption. Figure 10 shows powder XRD patterns of

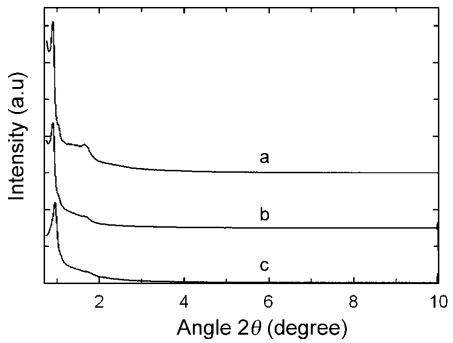


Figure 10. Powder XRD diffraction patterns of KIT-6-150 before and after lysozyme immobilization. a) Before adsorption. b) Initial concentration 2 g $L^{-1}$. c) Initial concentration 5 g $L^{-1}$ (solution pH 11, buffer concentration 25 mM).

KIT-6-150 before and after the adsorption experiment at initial lysozyme concentrations of 2 and 5 g $L^{-1}$ at pH 11. The shape of the XRD pattern of the lysozyme-loaded sample is similar to that of the parent KIT-6-150. This indicates that the structure of KIT-6-150 is retained even after immobilization of lysozyme molecules in the porous channels. However, the intensity of the lower angle peaks for the lysozyme-loaded sample is much lower than that of the sample before adsorption. The effect is even more prominent when a higher initial lysozyme concentration is used. The reduction in the intensity of the peaks is correlated with the increased amount of lysozyme adsorption in the pore channels, which gives a large contrast in density between the silica walls and the empty pores relative to that between the silica walls and the lysozyme molecules. These results also confirm that the lysozyme molecules are indeed adsorbed inside the mesochannels of KIT-6-150. Similar observations were also made for lysozyme immobilized on MCM-41, SBA-15, and mesoporous carbon.[36–39]

To quantify the degree of lysozyme immobilization in the mesochannels of KIT-6-150, a sample after the adsorption of lysozyme was analyzed by nitrogen adsorption measurements. Figure 11 shows the $N_2$ adsorption isotherms of KIT-6-150 before and after adsorption at lysozyme concentrations of 2 and 5 g $L^{-1}$. The amount of nitrogen adsorbed on KIT-6-150 decreases with increasing degree of lysozyme adsorption, and thus the specific pore volume is decreased from 1.53 to 0.31 $cm^3 g^{-1}$ on increasing the initial concentration of lysozyme from 2 to 5 g $L^{-1}$. From the structural parameters of lysozyme molecules we calculated that the volume of the lysozyme adsorbed (5 g $L^{-1}$) in the pores of KIT-6-150 is only 0.731 $cm^3$ g, which is 47.8% of the total free volume of KIT-6-150. However, a reduction of almost

  

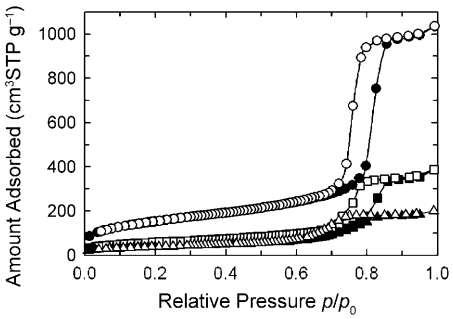


Figure 11. Nitrogen adsorption–desorption isotherms of KIT-6-150 before and after lysozyme immobilization (closed symbols: adsorption; open symbols: desorption): ● before adsorption, ■ initial concentration 2 g $L^{-1}$, ▲ initial concentration 5 g $L^{-1}$ (solution pH 11, buffer concentration 25 mM).

79.7% in the specific pore volume is observed for KIT-6-150 after adsorption in the nitrogen adsorption isotherm. As the XRD results reveal that the structural order of the materials is completely retained after protein immobilization, we surmise that the large difference between the calculated pore volume occupied by the adsorbed lysozyme molecule and the experimental data, which is almost 31.9%, is mainly due to hindered nitrogen adsorption in the lysozyme-filled pores of KIT-6-150 and not the result of some kind of structural deterioration after adsorption. From these results, we concluded that the lysozyme molecules are indeed tightly packed inside the mesochannels of KIT-6 materials.

The structural stability of lysozyme after adsorption inside the porous channels of KIT-6 was also analyzed by FTIR spectroscopy. The spectra were recorded for different amounts of lysozyme loaded on mesoporous KIT-6-150 and compared with the spectrum recorded for pure lysozyme (Figure 12). The band at 1245 $cm^{-1}$ (amide III band) can be

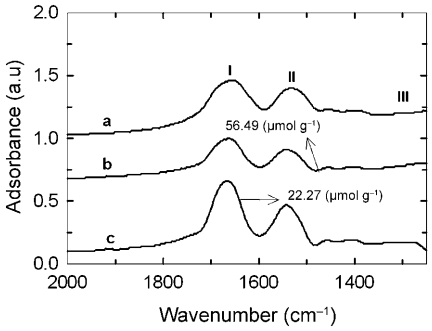


Figure 12. FTIR spectra of the pure lysozyme and different amounts of lysozyme loaded on KIT-6-150. a) Before adsorption. b) Initial concentration 2 g $L^{-1}$. c) Initial concentration 5 g $L^{-1}$ (solution pH 11, buffer concentration 25 mM).

assigned to β-sheet.[52–55] However, the amide III band is a very complex and depends on the force field, the nature of the side chains, and hydrogen bonding.[52] Moreover, the band also overlaps with the strong broad band for the Si-O-Si asymmetric stretching vibration. Thus, this band may not give useful information about the conformation of adsorbed lysozyme molecules. The spectra of the lysozyme-loaded samples show a sharp amide I band at 1542 $cm^{-1}$, which is attributed to the bending and stretching modes of the N–H and C–N groups, respectively.[55] The amide II band, which is observed at 1664 $cm^{-1}$, is attributed to C–O stretching of the α-helical confirmation of lysozyme molecules.[55] The presence and/or the position of these amide I and amide II bands, which are typically used for the determination of the confirmation and unfolding of the proteins, reveals that the denaturation of the protein secondary structure has not occurred and lysozyme molecules are highly stable even after immobilization inside the mesochannels.

## Conclusion

We have shown that KIT-6 materials with ultralarge pore diameter and high pore volume can be prepared by using pluronic P123 as surfactant and *n*-butanol as cosolvent at high synthesis temperatures. The materials were characterized by XRD and $N_2$ sorption. We have also demonstrated that the specific surface area, specific pore volume, and pore diameter of the materials can be finely tuned simply by adjusting the synthesis temperature. Among the KIT-6 materials, the material prepared at 150 °C, KIT-6-150, has a large pore diameter (11.3 nm) and a high specific pore volume (1.53 $cm^3 g^{-1}$). To the best of our knowledge, this is the first successful preparation of ultralarge-pore KIT-6 at a temperature around 150 °C. We also demonstrated for the first time the immobilization of lysozyme, which is a stable and hard protein, on KIT-6 materials with different pore diameters. The effect of the various adsorption parameters on lysozyme adsorption on KIT-6 materials were elucidated. The extent of adsorption mainly depends on solution pH, ionic strength, adsorption temperature, and pore volume and pore diameter of the adsorbent. The amount of lysozyme adsorbed on the large-pore KIT-6 is extremely high (57.2 μmol $g^{-1}$), and is much higher than that observed for MCM-41, SBA-15, KIT-5, mesoporous carbon, and carbon nanocage materials. We believe that the materials could also be used for adsorption and separation of large toxic biomolecules and dyes, and may also open the way for the fabrication of devices for chromatographic adsorption and separation process, and act as supports for the catalytic conversion of bulky organic molecules.

## Experimental Section

**Materials**: Hen egg white lysozyme (activity 25000 units $mg^{-1}$ of protein) was purchased from ICN biomedicals (Cataloge No. 100831) and used without further purification. Triblock copolymer pluronic P123 ($EO_{20}PO_{70}EO_{20}$, $M = 5800$) and *n*-butanol were obtained from Aldrich and used as a template and a cosolvent, respectively. Tetraethyl orthosilicate (TEOS) was used as a silica source and purchased from Aldrich.

**Syntheses of KIT-6 with different pore diameters**: KIT-6 with different pore diameters was synthesized by using P123/*n*-butanol mixture as struc-

  

ture-directing agent at different synthesis temperatures. In a typical synthesis, P123 (4 g) was dissolved in distilled water (144 g) and 35 wt% HCl solution (7.9 g). The mixture was stirred at 35 °C for 3 h. Then *n*-butanol (4.0 g) was added at once to the above mixture, which was continuously stirred at 35 °C for 1 h. Subsequently, TEOS (8.6 g) was added in one portion to the homogeneous clear solution and stirring was continued at 35 °C for 24 h. Then, the mixture was transferred to a polypropylene bottle and kept in an air oven at 100 °C for 24 h under static conditions. A set of KIT-6 materials was prepared by varying the synthesis temperature from 100 to 150 °C. The samples were labeled KIT-6-*x* where *x* denotes the synthesis temperature. Ryoo et al. reported the synthesis of KIT-6 materials by varying the temperature up to 130 °C.[44] However, in this case, the synthesis temperature was increased up to 150 °C, with the aim of obtaining KIT-6 with ultralarge pore diameter and large pore volume. The resultant product was collected by filtration while hot without washing and dried at 100 °C for 24 h in air. Finally, the material was calcined at 550 °C in air.

**Characterization**: The X-ray powder diffraction patterns of KIT-6 materials prepared at different temperatures were recorded on a Rigaku diffractometer with $Cu_{K\alpha}$ radiation ($\lambda = 0.154$ nm). The diffractograms were recorded in the $2\theta$ range of 0.8–10° with a $2\theta$ step size of 0.01° and a step time of 10 s. Nitrogen adsorption and desorption isotherms were measured at −196 °C on a Quantachrome Autosorb 1C analyzer. All the samples before protein adsorption were outgassed at 250 °C for 3 h prior to the nitrogen adsorption measurements, while the protein-loaded samples were outgassed at 40 °C for 24 h. The specific surface area was calculated by the BET method. The pore size distributions were obtained from the adsorption and desorption branch of the nitrogen isotherms by the Barrett–Joyner–Halenda method. HRTEM images were obtained with a TEM JEOL JEM-2000EX2. The preparation of samples for HRTEM analysis involved sonication in ethanol for 2–5 min and deposition on a copper grid. The accelerating voltage of the electron beam was 200 kV. FTIR spectra of KIT-6 before and after protein adsorption were recorded on a Nicolet Nexus 670 instrument by averaging 100 scans with a resolution of 2 $cm^{-1}$ in transmission mode by using the KBr self-supported pellet technique. The spectrometer chamber was continuously purged with dry air to remove water vapor.

**Lysozyme adsorption**: Lysozyme solutions with concentration ranging from 0.25 to 5 $g L^{-1}$ were prepared by dissolving different amounts of lysozyme in 10, 25, 50, and 100 mM buffer solutions (pH 6.5 potassium dihydrogenphosphate buffer, pH 9.6 and 10.5 sodium hydrogencarbonate buffer, and pH 12 disodium hydrogenphosphate buffer). The procedure for the adsorption experiments is as follows: the KIT-6 adsorbent (20 mg) was suspended in the respective lysozyme solutions (4 g) and the resulting mixtures were continuously shaken in an agitator at a speed of 160 shakes per minute at 20 °C until equilibrium was reached (typically 96 h for the different KIT-6 silica adsorbents used in this study). The amount of lysozyme adsorbed was calculated by UV absorption at 281.5 nm. Bulk adsorption experiments were also carried out with KIT-6-150 (100 mg), suspended in lysozyme solution (20 g) with two different concentrations (2 and 5 $g L^{-1}$).

## Acknowledgement

This work was financially supported by the Ministry of Education, Culture, Sports, Science and Technology (MEXT) under the Strategic Program for Building an Asian Science and Technology Community Scheme.

[1] V. Hladly, J. Bujis in *Biopolymers at Interfaces* (Ed.: M. Malmstem), Marcel Dekker, New York, **1985**.
[2] J. L. Brash, T. A. Horbett in *Proteins at Interfaces II: Fundamentals and Applications* (Eds.: J. L. Brash, T. A. Horbett), ACS symposium 602, American Chemical Society, Washington, DC, **1995**.
[3] J. D. Andrade in *Surface and Interfacial Aspects of Biomedical Polymers. Vol. 2: Protein Adsorption*, Plenum, New York, **1985**.
[4] C. Sandu, R. K. Singh, *Food Technol.* **1991**, *45*, 84.
[5] J. A. Hubbell, *BioTechnol.* **1995**, *13*, 565.
[6] M. Feng, A. B. Morales, T. Beugeling, A. Bantjes, K. Vanderwerf, G. Gosselink, B. Degrooth, J. Greve, *J. Colloid Interface Sci.* **1996**, *177*, 364.
[7] G. A. Rechnitz, *Chem. Eng. News* **1998**, *76*, 24.
[8] B. D. Martin, B. P. Gaber, C. H. Patterson, D. C. Turner, *Langmuir* **1998**, *14*, 3971.
[9] W. Inglish, G. H. Sander, P. M. Williamsan, M. C Davies, C. J. Roberts, S. J. B. Tendler, *Langmuir* **2001**, *17*, 7402.
[10] J. Deere, E. Magner, J. G. Wall, B. K. Hodnett, *J. Phys. Chem. B* **2002**, *106*, 7340.
[11] *Proteins at Interfaces: Physicochemical and Biochemical Studies* (Eds.: J. L. Brash, T. A. Horbett), American Chemical Society, Washington, DC, **1987**.
[12] J. D. Andrade, V. Hlady, *Adv. Polym. Sci.* **1986**, *79*, 1.
[13] K. Ishihara, H. Oshida, Y. Endo, T. Ueda, A. Watanabe, N. Nakabayashi, *J. Biomed. Mater. Res.* **1992**, *26*, 1543.
[14] A. M. Klibanov, *Science* **1983**, *219*, 722.
[15] H. H. Weetall, *Appl. Biochem. Biotech.* **1993**, *41*, 157.
[16] D. Avnir, S. Braun, O. Lev, M. Ottolenghi, *Chem. Mater.* **1994**, *6*, 1605.
[17] B. C. Dave, B. Dunn, J. S. Valentine, J. I. Zink, *Anal. Chem.* **1994**, *66*, 1120A.
[18] H. H. Weetall in *Analytical Uses of Immobilized Biological Compounds for Detection, Medical and Industrial Uses* (Eds.: G. G. Guilbault, M. Mascini), D. Reidel Publishing Co., Boston, MA, **1988**;1.
[19] M. Wahlgren, T. Arnebrant, I. Lundström, *J. Colloid Interface Sci.* **1995**, *175*, 506.
[20] T. J. Su, J. R. Lu, R. K. Thomas, Z. F. Cui, J. Penfold, *J. Colloid Interface Sci.* **1998**, *203*, 419.
[21] J. L. Robeson, R. D. Tilton, *Langmuir* **1996**, *12*, 6104.
[22] W. Norde, A. Anusiem, *Colloids Surf.* **1992**, *66*, 73.
[23] V. Ball, J. J. Ramsden, *J. Phys. Chem. B* **1997**, *101*, 5465.
[24] V. Ball, J. J. Ramsden, *Phys. Chem. Chem. Phys.* **1999**, *1*, 3667.
[25] V. Ball, J. J. Ramsden, *Colloids Surf. B* **2000**, *17*, 81.
[26] L. Moscou in *Introduction to Zeolites Science and Practice* (Eds: E. M. Flanigen, J. C. Jansen, H. van Bekkum), Elsevier, Amsterdam, **1991**, p. 1.
[27] B. Nagy, P. Bodart, I. Hannus, I. Kiricsi, *Synthesis,Characterization and Use of Zeolitic Microporous Materials*, DecaGen, Hungary, **1998**, p. 159.
[28] C. T. Kresge, M. E. Leonowicz, W. J. Roth, J. C. Vartuli, J. S. Beck, *Nature* **1992**, *359*, 710.
[29] D. Zhao, Q. Huo, J. Feng, B. F. Chmelka, G. D. Stucky, *J. Am. Chem. Soc.* **1998**, *120*, 6024.
[30] a) D. Zhao, J. Feng, Q. Huo, N. Melosh, G. Fredrikson, B. F. Chmelka, G. D. Stucky, *Science* **1998**, *279*; b) P. Yang, D. Zhao, D. Margolese, B. F. Chmelka, G. D. Stucky, *Nature* **1998**, *396*, 152.
[31] a) A. Vinu, V. Murugesan, M. Hartmann, *Chem. Mater.* **2003**, *15*, 1385; b) M. Hartmann, A. Vinu, *Langmuir* **2002**, *18*, 8010; c) A. Vinu, T. Krithiga, V. Murugesan, M. Hartmann, *Adv. Mater.* **2004**, *16*, 1817; d) A. Vinu, V. Murugesan, W. Bohlmann, M. Hartmann, *J. Phys. Chem. B* **2004**, *108*, 11496; e) A. Vinu, D. P. Sawant, K. Ariga, K. Z. Hossain, S. B. Halligudi, M. Hartmann, M. Nomura, *Chem. Mater.* **2005**, *17*, 5339; f) A. Vinu, P. Srinivasu, M. Miyahara, K. Ariga, *J. Phys. Chem. B* **2006**, *110*, 801; g) A. Vinu, K. Z. Hossain, G. Satish Kumar, K. Ariga, *Carbon* **2006**, *44*, 530; h) M. Hartmann, A. Vinu, G. Chandrasekar, *Chem. Mater.* **2005**, *17*, 829.
[32] Q. Huo. D. I. Margolese, U. Ciesla, D. G. Demuth, P. Feng, T. Gier, P. Sieger, A. Firouzi, B. F. Chmelka, F. Schuth, G. D. Stucky, *Chem. Mater.* **1994**, *6*, 1176.
[33] P. T. Tanev, T. J. Pinnavaia, *Science* **1995**, *267*, 865.
[34] J. F. Diaz, J. K. J. Balkus, *J. Mol. Catal. B* **1996**, *2*, 115.
[35] J. Deere, E. Magner, J. G. Wall, B. K. Hodnett, *Chem. Commun.* **2001**, 465.
[36] A. Vinu, V. Murugesan, M. Hartmann, *J. Phys. Chem. B* **2004**, *108*, 7323.

  

[37] A. Vinu, V. Murugesan, O. Tangermann, M. Hartmann, *Chem. Mater.* **2004**, *16*, 3056.
[38] a) A. Vinu, M. Miyahara, K. Ariga, *J. Phys. Chem. B* **2005**, *109*, 6436; b) A. Vinu, C. Streb, V. Murugesan, M. Hartmann, *J. Phys. Chem. B* **2003**, *107*, 8297.
[39] A. Vinu, M. Miyahara, V. Sivamurugan, T. Mori, K. Ariga, *J. Mater. Chem.* **2005**, *15*, 5122.
[40] A. Vinu, M. Hartmannm, *Stud. Surf. Sci. Catal.* **2004**, *154*, 2987.
[41] M. Miyahara, A. Vinu, H. Z. Hossain, T. Nakanishi, K. Ariga, *Thin Solid Films* **2006**, *499*, 13.
[42] M. Miyahara, A. Vinu, K. Ariga, *Mater. Sci. Eng. C* **2007**, *27*, 232.
[43] A. Vinu, M. Miyahara, K. Z. Hossain, M. Takahashi, V. V. Balasubramanian, T. Mori, K. Ariga, *J. Nanosci. Nanotechnol.* **2007**, *7*, 828.
[44] T. W. Kim, F. Kleitz, B. Paul, R. Ryoo, *J. Am. Chem. Soc.* **2005**, *127*, 7601.
[45] a) C. C. F. Blake, D. F. Koenig, G. A. Mair, A. C. T. North, D. C. Phillips, V. R. Sarma, *Nature* **1965**, *206*, 757; b) Q. Garrett, R. W. Garrett, B. K. Milthorpe, *Invest. Ophth. Vis. Sci.* **1999**, *40*, 897; c) R. E. Canfield, A. K. Liu, *J. Biol. Chem.* **1965**, *240*, 2000; d) D. P. Kharakoz, A. P. Sarvazyan, *Biopolymers* **1993**, *33*, 11; e) K. P. Wilson, B. A. Malcolm, B. W. Matthews, *J. Biol. Chem.* **1992**, *267*, 10842.
[46] C. Giles, T. McEvan, S. Nakhwa, D. Smith, *J. Chem. Soc.* **1960**, 3973.
[47] G. Jackler, R. Steitz, C. Czeslik, *Langmuir* **2002**, *18*, 6565.
[48] W. Norde, A. C. I. Anustem, *Colloids Surf.* **1992**, *66*, 73.
[49] T. Arai, W. Norde, *Colloids Surf.* **1990**, *51*, 1.
[50] K. A. Dill, *Biochemistry* **1999**, *29*, 7133.
[51] W. Norde, *Adv. Colloid Interface Sci.* **1986**, *25*, 267.
[52] W. Hammond, E. Prouzet, S. D. Mahanti, T. Pinnavaia, *Microporous Mesoporous Mater.* **1999**, *27*, 19.
[53] X. S. Zhao, F. Adusley, G. Q. Lu, *J. Phys. Chem. B* **1998**, *102*, 4143.
[54] S. Adams, A. M. Higgins, R. A. L. Jones, *Langmuir* **2002**, *18*, 4854.
[55] F. M. Fu, D. B. DeOliveira, W. R. Trumble, H. K. Sarkar, B. R. Singh, *Appl. Spectrosc.* **1994**, *48*, 1432.

Received: June 30, 2008
Published online: November 12, 2008

  